Cerebral Cortex, July 2016;26: 3260–3272

doi: 10.1093/cercor/bhw066
Advance Access Publication Date: 14 March 2016
Original Article

ORIGINAL ARTICLE

Plasticity-Related Gene 1 Affects Mouse Barrel Cortex Function via Strengthening of Glutamatergic Thalamocortical Transmission

Petr Unichenko[1], Sergei Kirischuk[1], Jenq-Wei Yang[1], Jan Baumgart[2], Thomas Roskoden[3], Patrick Schneider[3], Angela Sommer[3], Guilherme Horta[2], Konstantin Radyushkin[4], Robert Nitsch[2], Johannes Vogt[2] and Heiko J. Luhmann[1]

[1]Institute of Physiology, University Medical Center of the Johannes Gutenberg University Mainz, D-55128 Mainz, Germany, [2]Institute for Microanatomy and Neurobiology, University Medical Center of the Johannes Gutenberg University Mainz, Langenbeckstrasse 1, Building 708, D-55131 Mainz, Germany, [3]Institute of Anatomy, Otto-von-Guericke-University of Magdeburg, Leipziger Str. 44, D-39120 Magdeburg, Germany and [4]Focus Program Translational Neuroscience, University Medical Center of the Johannes Gutenberg-University, Mainz, Germany

Address correspondence to Heiko J. Luhmann, Institute of Physiology, University Medical Center of the Johannes Gutenberg University Mainz, Duesbergweg 6, D-55128 Mainz, Germany. Email: luhmann@uni-mainz.de

Petr Unichenko, Sergei Kirischuk, and Jenq-Wei Yang contributed equally.

Johannes Vogt and Heiko J. Luhmann contributed equally as last authors.

Abstract

Plasticity-related gene-1 (PRG-1) is a brain-specific protein that modulates glutamatergic synaptic transmission. Here we investigated the functional role of PRG-1 in adolescent and adult mouse barrel cortex both in vitro and in vivo. Compared with wild-type (WT) animals, PRG-1-deficient (KO) mice showed specific behavioral deficits in tests assessing sensorimotor integration and whisker-based sensory discrimination as shown in the beam balance/walking test and sandpaper tactile discrimination test, respectively. At P25-31, spontaneous network activity in the barrel cortex in vivo was higher in KO mice compared with WT littermates, but not at P16-19. At P16-19, sensory evoked cortical responses in vivo elicited by single whisker stimulation were comparable in KO and WT mice. In contrast, at P25-31 evoked responses were smaller in amplitude and longer in duration in WT animals, whereas KO mice revealed no such developmental changes. In thalamocortical slices from KO mice, spontaneous activity was increased already at P16-19, and glutamatergic thalamocortical inputs to Layer 4 spiny stellate neurons were potentiated. We conclude that genetic ablation of PRG-1 modulates already at P16-19 spontaneous and evoked excitability of the barrel cortex, including enhancement of thalamocortical glutamatergic inputs to Layer 4, which distorts sensory processing in adulthood.

Key words: behavior, in vitro, in vivo, network activity, patch-clamp recordings

Introduction

The whiskers of rodents are somatotopically represented in the primary somatosensory (barrel) cortex (for review, Feldmeyer et al. 2013). Sensory information from the whiskers is transferred through the brain stem and thalamus to Layer 4 neurons in the barrel cortex, and the thalamocortical input to Layer 4 neurons is the main pathway for sensory information to the barrel cortex. A remarkable activity-dependent refinement of this input occurs during early postnatal development (for review, Feldman et al. 1999; Daw, Scott, et al. 2007). There is substantial evidence that N-methyl-D-aspartate (NMDA) receptor-dependent synaptic plasticity is required for receptive field formation and refinement (Fox et al. 1996). Obviously, glutamate release required to activate postsynaptic NMDA receptors on Layer 4 neurons depends both on activity of thalamic neurons and on release probability at thalamocortical presynapses. The latter can be potentiated or suppressed via activation of different presynaptic receptors (for review, Malenka 2003).

Recently, a new class of integral membrane proteins, named plasticity-related genes (PRGs), has been discovered (Brauer et al. 2003). PRGs possess homology to lipid phosphate phosphatases (LPPs) and can interact with lysophosphatidic acid (LPA), a well-described bioactive phospholipid, which modulates various cellular functions, including cell proliferation, migration, and cortical morphogenesis (Fukushima et al. 2002; Kingsbury et al. 2003; van Leeuwen et al. 2003).

PRG-1 expression was exclusively observed in glutamatergic neurons in a variety of brain structures, including hippocampus and neocortex of rodents and humans (Trimbuch et al. 2009; Tokumitsu et al. 2010; Vogt et al. 2015). Intracellularly, PRG-1 is located at the postsynaptic density of glutamatergic synaptic contacts, but is absent in presynaptic structures or at GABAergic synapses (Trimbuch et al. 2009; Tokumitsu et al. 2010). This specific localization of PRG-1 enables PRG-1 to play an important role in controlling glutamatergic synaptic transmission. Genetic deletion of the *prg1* gene leads to an increase of both amplitude of evoked excitatory postsynaptic currents (EPSCs) and frequency of miniature EPSCs in hippocampal CA1 neurons, whereas inhibitory postsynaptic currents (PSCs) are not affected. As expected, this selective potentiation of glutamatergic transmission resulted in hyperexcitability. Electrographic ictal events and epileptic seizures were observed in about 50% of the PRG-1-KO mice starting around postnatal day (P) 20. Moreover, all PRG-1-KO mice exhibiting epileptic seizures died during status epilepticus (Trimbuch et al. 2009). Similarly, a single-nucleotide polymorphism in prg-1 has been recently shown to affect the E/I balance and lead to an impaired sensory gating (Vogt et al. 2015). However, the functional role of the PRG-1/LPA pathway in brain development and neuronal plasticity is not fully understood.

Non-epileptic PRG-1-KO animals show only hippocampal hypersynchronized activity, but no ictal events or seizures (Trimbuch et al. 2009). These mice remain seizure-free allowing further behavioral and electrophysiological studies to elucidate the mechanisms underlying neuronal hyperexcitability in more mature PRG-1-KO animals. Since our studies show that PRG-1 is strongly expressed in Layer 4 of the murine cerebral cortex (Vogt et al 2015; see Supplementary Fig. 1) and previous studies focused on hippocampal function, it is of central interest to investigate the role of PRG-1 in the cerebral cortex and in sensory processing.

Here we addressed the questions whether genetic ablation of the *prg-1* gene 1) influences sensory integration in adult animals and 2) affects neuronal activity in the adolescent barrel cortex both in vivo and in vitro. We found that PRG-1-KO mice show a deficiency in whisker-related sensory perception as revealed by the sandpaper maze test. Genetic knockout of *prg-1* strongly facilitates spontaneous network activity both in vivo and in vitro, although at different time points during development. Experiments performed in thalamocortical slices showed that glutamatergic thalamocortical inputs are potentiated in PRG-1-KO mice compared with WT littermates already at P16-19, while evoked cortical responses elicited by single whisker stimulation in vivo are facilitated only at P25-31. Thus, PRG-1 is important for the activity-dependent development and tuning of the somatosensory system.

Materials and Methods

All experiments were conducted in accordance with the national laws for the use of animals in research (the European Communities Council Directive of 24 November 1986 (86/609/EEC)) and approved by the local ethical committee (Landesuntersuchungsamt Rheinland-Pfalz 23.177-07/G 10-1-010 and Landesuntersuchungsamt Sachsen-Anhalt 42502-2-1114UniMD). Experiments were designed to minimize the number of animals used and their suffering. Breeding of heterozygous PRG-1 animals (Trimbuch et al. 2009) allowed the analyses of wild-type and PRG-1-KO mice from the same litter.

Behavioral Studies

For the beam balance/walking test and for the Rota-Rod test, adult female PRG-1 knockout (KO) and female wild-type (WT) littermates were assessed. Mice were singly housed in transparent cages and maintained on a 12/12 h light/dark cycle with food and water ad libitum. All tests were performed during the light phase. Fine motor coordination, which includes somatosensory integration, was tested using the beam balance/walking test, while motor performance was assessed using the Rota Rod test. The beam balance/walking test was performed on an elevated narrow beam where mice had to remain upright and to walk. The beam was located 36 cm above the floor with small platforms on each end. Animals were successively tested on 3 different beams with a width of 20, 10, and 5 mm and a length of 700 mm. Mice were placed in the middle of the beam, and a run was stopped if mice reached a platform with all 4 feet or after 180 s. Animals had a 30-min break between runs. We analyzed total time, length of a run, the numbers of faults such as slides or falls, and numbers of turns. Slides during the beam walk were counted when the mice slipped off at the side of the beam with 1 limb at least.

In the Rota Rod test, mice have to maintain balance and keep pace with a rotating rod. The Rota Rod treadmill apparatus (New Rota-Rod for Mice, Ugo Basile, Varese, Italy) was divided into 5 separated testing stations. One day before testing, mice were habituated on the apparatus. The animals had to run for 1 min at a speed of 4 rounds/min (rpm) and of 10 rpm with a break of 5 min between the trials. The test run was accelerated from 4 to 40 rpm within 5 min. The total running time and the rpm were manually registered when the mice fell down. Alternatively the run was stopped after 300 s at 40 rpm. The test was performed 3 times with a break of 30 min between the runs.

The sandpaper tactile discrimination test was designed to assess for behavioral deficits in processing of somatosensory whisker-related information (Morita et al. 2011). To avoid bias by visual and/or olfactory cues, animals were tested in the dark (0.7 Lux), and food pellets (accessible and non-accessible) were deposited in all arms. Briefly, we used a reward-based strategy

in the 8-arm maze, where mice had to discriminate surface roughness to get reward—chocolate-flavored sweet food pellet. To provide required level of motivation, mice were first food deprived reducing their body weight to 80% of initial body weight (Rowland 2007), which was maintained during the whole experiment. Water was freely available during food deprivation period. After habituating mice (males or mixed gender) with chocolate-flavored food pellets for 1 h daily for 7 days, animals were habituated for 7 days in the 8-arm maze (10 min daily), where pellets were available at the end of each arm. At the end of maze habituation, all mice showed no signs of anxiety in the maze, moved freely and consumed not <40 pellets within 10 min. For the discrimination task, we used 2 different grades of sandpaper (P60 and P80, Bosch): P60 (coarse) being with bigger sand particle size than P80 (fine). The inner side walls of the arms were covered with sand paper: 4 arms with P60 and other 4 with P80. To prevent animals from learning the alternate-visiting strategy, arms of the 8-arm radial maze were arranged in the following fashion: P60-P60-P80-P60-P80-P60-P80-P80. The arms with P60 sandpaper were all rewarded with pellets in the end of the arms. The bulk of non-accessible food pellets was placed behind a wire mesh at the end of each arm to prevent animals to use a pellet scent as a cue. Each animal was tested for 10 min. The number of correct (if animal entered P60 arm) and incorrect visits was manually scored. The criterion to score for the visit was when the animal passed at least three-fourths of the arm length.

Surgical Preparation, In Vivo Electrophysiological Recordings, and Their Analysis

Extracellular in vivo recordings were performed in the barrel cortex of 2 age groups at postnatal days (P) P16–19 and P25–31, both in WT and in KO mice (Yang et al. 2009). Under initial intraperitoneal urethane anesthesia (1.6–2 g/kg, Sigma-Aldrich), the head of the mouse was fixed and the bone, but not the dura mater, above the barrel cortex was carefully removed. Animals were kept at a constant temperature of 37 °C by placing them on a heating blanket. During recording, additional urethane (10–20% of the initial dose) was given when the mice showed any sign of distress. In P16–19 WT and KO mice, a 4-shank 80-channel electrode (150 µm horizontal shank distance and 50 µm vertical inter-electrode distance, 1–2 MΩ, NeuroNexus Technologies, Ann Arbor, MI, USA) was inserted perpendicularly into the barrel cortex to obtain field potential and multi-unit activity (MUA) recordings. In P25–31 WT and KO mice, a 4-shank 16-channel electrode (125 µm horizontal shank distance and 50 µm vertical inter-electrode distance, 1–2 MΩ, NeuroNexus Technologies) was inserted perpendicularly into the barrel cortex and the electrode recording sites were located from 200 to 400 µm depth. Sixty to 90 min after electrode insertion, single whisker stimulation was performed to identify the corresponding cortical representation (see Supplementary Fig. 2*A*,*B*). A single whisker was stimulated approximately 1 mm from the snout using a miniature solenoid actuator (modified from Krupa et al. 2001) that generated for 16 ms a deflection in the rostral-to-caudal direction.

Data were imported and analyzed offline using MATLAB software version 7.7 (MathWorks). We computed current source density (CSD) map using averaged evoked local field potential (LFP). First, we duplicated the LFP traces in uppermost and lowermost channels of each shank. One-dimensional CSD profiles were then calculated from the LFP according to a 3-point formula (Freeman and Nicholson 1975). The CSD values I_m were derived from the second spatial deviation of the extracellular field potentials f and calculated by the finite-difference formula

$$I_m = -\frac{[f(x-h) - 2f(x) + f(x+h)]}{h^2},$$

where h is the distance between successive measuring points (50 µm in the present investigation) and x is the coordinate perpendicular to the cortical layer. In the CSD profiles, current sinks are indicated by downward deflections and sources by upward deflections. To facilitate visualization of CSD profiles, we generated color image plots by linear interpolation along the depth axis. The blue color represented current sinks and red color represented current sources (see Supplementary Fig. 2*C*).

In P16–19 WT and KO mice, cortical layers were functionally identified according to the evoked CSD profile. The channel with the maximal response amplitude to each principle whisker stimulation was always located in Layer 4 and was chosen for further analysis (see Supplementary Fig. 2*C*,*D*). In P25–31 WT and KO mice, a 4-shank 16-channel electrode recorded cortical activity in 200–400 µm depth, which included Layer 4.

In each experiment, 30 min continuous recording of spontaneous extracellular LFP was used to analyze the mean fast Fourier transform (FFT). The 30 min LFP recording was separated into 360 segments, that is, each segment contained 5 s LFP recording. Next, FFT analysis was applied (the frequency resolution was 0.2 Hz), and the mean FFT was calculated by averaging the FFT spectra in all 360 segments. MUA was detected in 800–5000 Hz filtered LFP signals by applying a threshold at 7.5 times the baseline standard deviation (SD). A MUA burst was defined as a spike train consisting of at least 10 spikes with an inter-spike interval shorter or equal than 33 ms.

At the end of each experiment, animals were killed with an overdose of ketamine (240 mg/kg) and xylazine (31 mg/kg) and perfused with sodium phosphate buffer and fixed with 4% paraformaldehyde. The mouse brain was tangentially sectioned at 200 µm thickness and processed for cytochrome oxidase histochemistry to identify the barrel(s) from which signals were recorded (see Supplementary Fig. 2*B*).

Thalamocortical Brain Slice Preparation

Thalamocortical slices of 350 µm thickness were prepared from P16–19 WT and KO mice as described elsewhere (Agmon and Connors 1991; Schubert et al. 2003; Staiger et al. 2004). Briefly, animals were anesthetized with isofluorane and decapitated. Brains were rapidly removed and transferred into ice-cold artificial cerebrospinal fluid (ACSF) that contained (in mM): 126 NaCl, 2.5 KCl, 10 glucose, 1.25 NaH_2PO_4, 26 $NaHCO_3$, 2 $CaCl_2$, and 1 $MgCl_2$ constantly bubbled with 5% CO_2/95% O_2 (pH = 7.3). Paracoronal slices were prepared at an angle of 55° relative to the middle on a ramp at an angle of 13° using a vibratome (Campden Instruments Ltd, UK). After preparation slices were stored for at least 1 h at room temperature in ACSF. The pH was buffered to 7.3 by continuous bubbling with a 5% CO_2/95% O_2.

For recordings, slices were placed into a recording chamber (~0.4 mL volume) on the microscope stage (Axioscope FS, Zeiss, Oberkochen, Germany). Slices were submerged with a constant flow of oxygenated ACSF. Flow rate was set to 1 mL/min. All experiments were performed at 31–32 °C. The somatosensory cortex was identified by the presence of barrels using low magnification objective (×5; see Supplementary Fig. 3*A*). Whole-cell voltage-clamp recordings were performed from spiny stellate neurons in Layer 4 of the barrel cortex using phase-contrast

optics. A ×40 water immersion objective (Zeiss, Oberkochen, Germany) was used in all experiments. For recordings, borosilicate glass electrodes were used and filled with (in mM) 110 potassium gluconate, 20 KCl, 5 NaCl, 0.5 $CaCl_2$, 5 EGTA, 20 HEPES, 2 MgATP, 0.3 GTP, pH was set to 7.2 with KOH. Electrode resistance was 3–5 MΩ. Electrophysiological signals were acquired using an EPC-10 amplifier and TIDA 5.24 software (HEKA Elektronik, Lambrecht, Germany). The signals were filtered at 3 kHz and sampled at a rate of 10 kHz. Hyperpolarizing pulses of 10 mV were used to control access resistance. Only recordings with a series resistance below 40 MΩ were accepted. Series resistance compensation was not applied. Cells exhibiting more than 20% changes in access resistance during an experiment were discarded. The holding potential was set to −70 mV. Miniature EPSCs (mEPSCs) were recorded in the presence of tetrodotoxin (TTX, 0.5 µM), a blocker of voltage-gated Na^+ channels, and gabazine (10 µM), an antagonist of $GABA_A$ receptors. TTX and gabazine were obtained from Tocris (Bristol, UK). All other chemicals were obtained from Sigma-Aldrich.

Evoked EPSCs (eEPSCs) were elicited at a frequency of 0.1 Hz using a bipolar tungsten electrode placed in the ventral posteriomedial nucleus (VPM) of the thalamus. An isolated stimulation unit (A365, World Precision Instruments, Sarasota, USA) was used to generate rectangular electrical pulses. Pulse duration was set to 0.2 ms. Pulse intensity was adjusted to activate a unitary synaptic input (minimal stimulation) and typically amounted to 10–30 µA. Stimulation was accepted as minimal if eEPSCs occurred at short and constant latency (<3.5 ms), demonstrated paired-pulse depression and showed no decrease in latency of the second eEPSC induced 50 ms after the first response (Beierlein et al. 2003; Kirmse et al. 2007). In addition, eEPSCs were inspected at a holding potential of −50 mV, the Nernst Cl^- reversal potential. Depolarizing eEPSCs recorded at this membrane potential confirmed the glutamatergic nature of the evoked signals.

In Utero Electroporation

In utero electroporation was performed as described before (Trimbuch et al. 2009). Briefly, chronologically mated mice (E13.5 determined by the appearance of the vaginal plug) were anesthetized by inhalation of an isoflurane-air mix and the uterine horns were exposed. The DNA solution (1–1.5 µL/embryo) was injected through the uterine wall into the lateral ventricle of the embryos by pulled glass capillaries (World Precision Instruments). Electric pulses were delivered to embryos by holding the injected brain through the uterine wall with forceps-type electrodes (CUY650P5) connected to a square–pulse generator (CUY21SC, Nepa Gene Co., Ichikawa City, Chiba, Japan). Five 35 V pulses of 50 ms duration were applied at 1 Hz. The uterine horns were carefully put back into the abdominal cavity before the muscle wall and skin were stitched. The use of this method in PRG-1 KO animals allowed us to directly investigate the effect of PRG-1 in reconstituted single neurons embedded in a PRG-1-deficient environment. These circumstances enabled us to directly analyze PRG-1 action from the postsynaptic compartment without bias, which can be derived from general network effects or from input of distant brain regions. Neurons transfected using in utero electroporation approach were identified in acute brain slices by green (green fluorescent protein, GFP) fluorescence. In rescue experiments, mEPSCs were recorded alternatively from GFP-positive and GFP-negative spiny stellate neurons in each brain slice used.

Data Evaluation and Statistics

Statistical analyses of behavioral and in vivo data were performed with GraphPad Prism (GraphPad Software, Inc., La Jolla, CA, USA). All stochastically independent samples were compared using the Student *t*-test or 1-way ANOVA followed by post hoc Tukey's multiple comparison test for normal distributed values or the Mann–Whitney test for values displaying a nonparametrical distribution. Normal distribution was assessed using the Kolmogorov–Smirnov test. For comparison of WT and PRG-1 KO animal behavior over time and between genotypes, groups were analyzed using a 2-way ANOVA. In vitro data were evaluated using TIDA 5.24 (HEKA Elektronik). mEPSCs were analyzed using PeakCount V3.2 software (C. Henneberger, Institute of Neurophysiology, Charité, Berlin). The program employs a derivative threshold-crossing algorithm to detect individual EPSCs. Each automatically detected event was displayed for visual inspection. Differences between means (in vitro data) were tested for significance using unpaired Student's *t*-test.

Results

PRG-1 Genetic Deletion Affects Sensorimotor Integration and Sensory Perception

Firstly, we have investigated the effects of PRG-1 genetic deletion on sensorimotor function. Adult WT and PRG-1-KO mice were tested in the beam balance/walking test on 3 different beams with a diameter of 20, 10, and 5 mm. Here, PRG-1-KO mice displayed significantly more slides compared with WT littermates (KO 10.8 ± 1.8, $n = 18$; WT 5.4 ± 1.1, $n = 18$, $P < 0.01$, Fig. 1*A*). This sensorimotor deficit in the KO mice was even more obvious when the number of slides was calculated per 100 cm walking distance (KO 56.9 ± 14.3; WT 8.9 ± 1.3; $P < 0.001$, Fig. 1*B*). In accordance with lower sensorimotor performance, PRG-1-KO mice displayed more turns (KO 8.2 ± 1.2; WT 4.5 ± 1.0, $P < 0.05$, Fig. 1*C*) and had a significantly lower overall advance speed (KO 48 ± 11 cm/min; WT 90 ± 13 cm/min, $P < 0.05$, Fig. 1*D*). The difference was most evident on the 5 mm wide beam (KO 39 ± 14 cm/min; WT 102 ± 22 cm/min, $P < 0.01$). However, the overall run length was not different in PRG-1-KO mice, which displayed even a significantly longer running time on the 5 mm wide beam (Fig. 1*E*,*F*), which argues against a lower general activity or an avoidance of the beam walk in these mice.

To assess possible basic motor coordination deficits, which could bias the observed results in the beam balance/walking test, the motor performance of PRG-1-KO mice and WT litters was assessed in the Rota Rod test, which is a sensitive test to observe simple coordinated motor skills (Crawley and Paylor 1997; Shiotsuki et al. 2010). Both the total running time (KO 235 ± 15 s, $n = 18$; WT 179 ± 13 s, $n = 18$, $P < 0.05$; not shown) and speed of the rod at fall (KO 32 ± 2 rpm; WT 26 ± 2 rpm; $P < 0.01$) were higher in KO mice compared with WT animals (Fig. 1*G*). While 13 out of 18 PRG-1-KO mice were able to stay on average more than 200 s on the rotating roll, only 4 out of 18 WT were able to a similar performance. Other behavioral variables and body weight (KO 24.1 ± 0.6 g; WT 24.4 ± 0.6 g) were not different between both genotypes in adult animals. These results suggest that performance differences in the beam balance/walking test most probably reflect deficits in sensory integration rather than pure motor abilities of PRG-1-KO mice.

Since behavioral results point to an altered sensorimotor integration, we directly assessed whisker-mediated sensory perception in adult WT and PRG-1 KO mice. Whisker-mediated

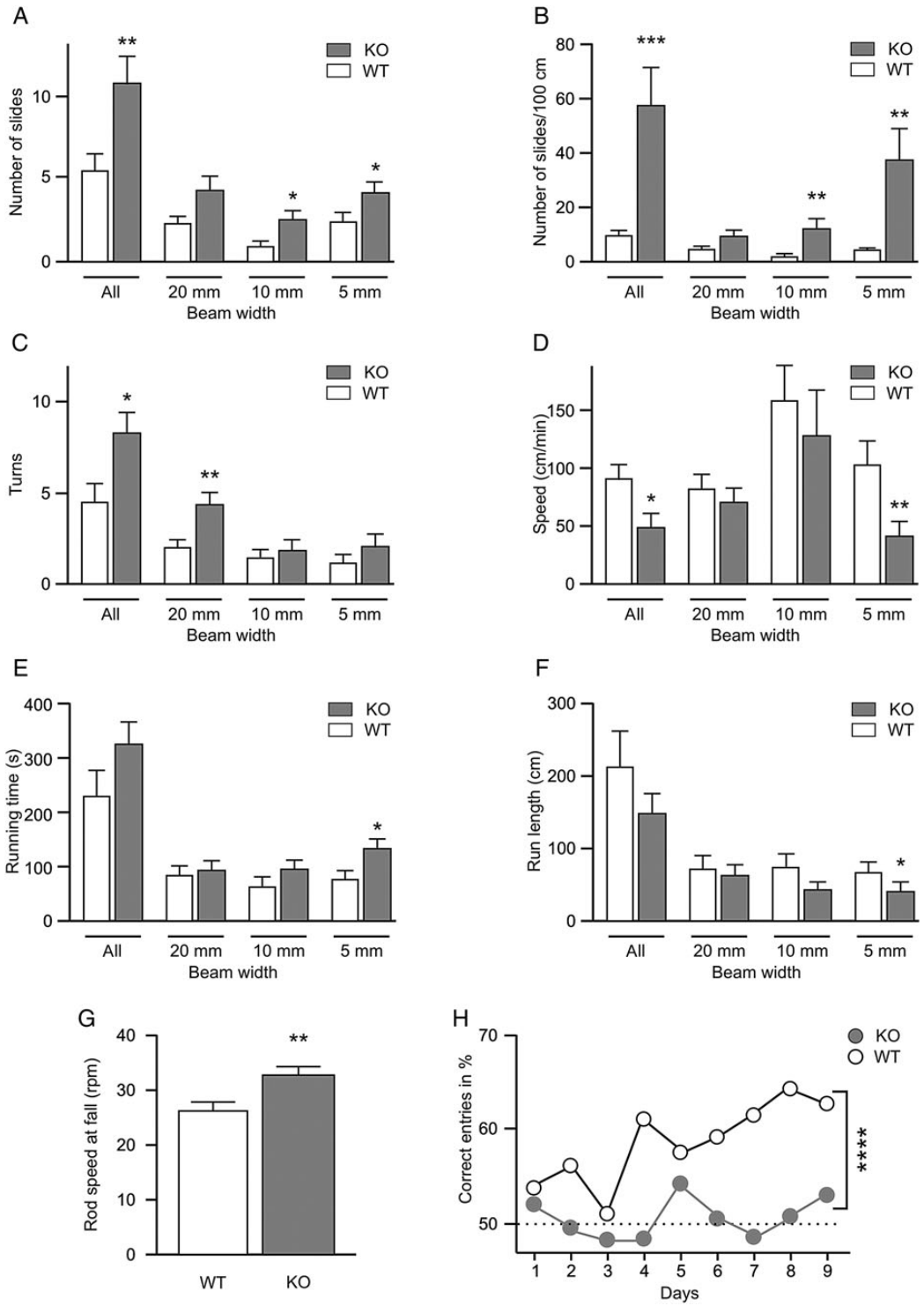

Figure 1. Behavioral assessment of sensorimotor integration and whisker-mediated sensory perception. (*A–F*) Bar diagrams demonstrating quantitative differences in the beam-walking test performance between PRG-1-KO (KO, gray columns) mice ($n = 18$) and wild-type (WT, open columns) littermates ($n = 18$). The following parameters have been assessed: number of slides (*A*), mean number of slides per 100 cm (*B*), number of turns (*C*), running speed (*D*), running time (*E*), and path length (*F*). Results show mice performance on 20, 10, and 5 mm wide beams during 180 s and summary of all beams (all). (*G*) Bar diagrams demonstrating quantitative differences in the Rota Rod test performance between PRG-1-KO (KO, grey columns) mice ($n = 18$) and wild-type (WT, open columns) littermates ($n = 18$) in terms of speed at the time of fall. Data were obtained from 3 trials per mouse. (*H*) Mouse performance in a sandpaper maze designed to assess whisker-mediated sensory perception. While WT animals improved over time ($n = 7$ WT mice), PRG-1 KO mice did not improve above chance levels ($n = 12$ PRG-1 KO mice; performance over time and between groups was calculated using a 2-way ANOVA). Values represent mean ± SEM. Asterisks mark statistically significant differences, $^{*}P < 0.05$, $^{**}P < 0.01$, $^{***}P < 0.001$, and $^{****}P < 0.0001$.

perception in mice is well described (Morita et al. 2011) and was shown to be specifically processed in the primary somatosensory barrel cortex (Garion et al. 2014). For assessing whisker-mediated sensory perception, we used a simplified maze, where arms were covered with sandpaper of 2 different grades (60 grade with a grain size of 265 µm and 80 grade with a grain size of 190 µm). Only arms with 1 sandpaper grade (60 grade sandpaper) were rewarded by accessible food pellets while food pellets were not accessible in other arms (covered with 80 grade sandpaper). Since experiments were performed in darkness, animals could only orient by whisker-based texture discrimination. While WT mice were able to discriminate between these 2 sandpaper grades and significantly improved over time, PRG-1 KO mice did not improve remaining even after 9 days of continuous training at chance levels (Fig. 1*H*). In sum, our results show that PRG-1 KO mice display a significant disturbance in processing of sensory stimuli. Therefore, we next analyzed in more detail the somatosensory cortex using in vivo and in vitro electrophysiological recordings.

PRG-1 Ablation Influences Spontaneous Neuronal Activity in the Somatosensory Cortex In Vivo

PRG-1-KO mice start to exhibit hypersynchronized neuronal activity in vivo at around P20 (Trimbuch et al. 2009). Therefore, to study the role of PRG-1 in the functional maturation of the somatosensory system, neuronal activity in the barrel cortex of PRG-1-KO mice and WT littermates was recorded under urethane anesthesia at P16–19, that is, before the onset of hyperactivity, and at P25–31.

To address the question whether PRG-1 influences intracortical network activity, we first recorded LFPs in the barrel cortex of WT and KO mice in vivo. Figure 2 shows the characteristic spontaneous and MUA recorded in WT and PRG-1-KO littermates at P16–19 (Fig. 2*A*1) and P25–31 (Fig. 2*B*1). To quantify the data, we first applied a fast Fourier transformation (FFT) and compared the corresponding power spectra between WT and PRG-1-KO mice. Figures 2*A*2 and 3 show that at P16–19 spontaneous activity in PRG-1-KO mice displayed a significantly lower power in all frequency bands of the FFT spectrum. In contrast, at P25–31 power spectra of spontaneous activity were higher in PRG-1-KO animals compared with WT littermates, but this difference was significant only in the β and γ frequency bands (Figs 2*B*2 and 3). Interestingly, no significant difference in any frequency band was observed between the P16–19 and P25–31 age group in WT animals (all $P > 0.2$), indicating that PRG-1 deletion leads to a potentiation of spontaneous synchronized activity in the somatosensory barrel cortex between P16–19 and P25–31.

To substantiate these results, we analyzed MUA in WT and PRG-1-KO littermates at P16–19 and P25–31. In agreement with the above data, both MUA firing rate and the number of MUA bursts were lower in PRG-1-KO mice compared with WT littermates at P16–19. At P25–31, MUA firing rate was significantly higher in PRG-1-KO animals (Fig. 3*A*,*B*), whereas no difference was observed between MUA activity in P16–19 and P25–31 WT mice. These data are in good agreement with the Fourier spectra analyses of the spontaneous LFP recordings (Fig. 2) and indicate that PRG-1 deletion results in a developmental boost of spontaneous activity in the barrel cortex between P16–19 and P25–31. Interestingly, the MUA burst duration was significantly longer in P16–19 PRG-1-KO mice compared with P25–31 WT animals, suggesting that PRG-1 ablation appears to lead to a more prolonged synchronization of spontaneous activity in the barrel cortex already at P16–19 (Fig. 3*C*).

PRG-1 Deletion Affects Sensory-Evoked Responses in the Somatosensory Cortex In Vivo

As PRG-1 deletion affects spontaneous network synchronization, next we addressed the question whether lack of PRG-1 also influences evoked responses in the barrel cortex in vivo. LFP responses in neocortical Layer 4 were elicited by single whisker stimulation. Figure 4*A*–*C* shows that both amplitudes and slopes of evoked LFPs in the whisker-related cortical column were not significantly different between WT and PRG-1-KO animals at P16–19. In contrast, at P25–31 amplitudes and slopes of evoked responses were smaller in WT mice compared with PRG-1-KO littermates. In parallel, a significant increase of evoked response duration was observed in P25–31 WT mice, but not in PRG-1-KO litters (Fig. 4*D*). These data were supported by measurements of the peak amplitudes, slopes, and durations of the current sinks in the CSD analyses (Fig. 4*E*–*H*). Thus, we conclude that between P16–19 and P25–31 sensory-evoked responses become smaller in amplitude and longer in duration during normal physiological development, that is, in WT animals. However, this process is impaired in PRG-1-KO mice.

Next we studied the properties of short-term synaptic plasticity in WT and PRG-1-KO mice at P16–19 and P25–31 by application of a paired-pulse stimulation protocol. A single whisker was stimulated twice at inter-stimulus intervals (ISIs) of 100 or 250 ms. No difference in paired-pulse ratio (S2/S1 ratio) was observed between WT and PRG-1-KO mice in both age groups tested (Fig. 5). The S2/S1 ratio showed a developmental increase in WT and PRG-1-KO mice.

In summary, our in vivo data demonstrate that genetic deletion of *prg-1* causes a reduction in spontaneous network activity at P16–19, which is over-compensated within the next approximately 10 days leading to a neuronal hyperexcitability at P25–31. In addition to this boosting of spontaneous network activity in PRG-1-KO mice during the third and fourth postnatal week, PRG-1 loss prevents a developmental change in the responsiveness to sensory stimulation.

PRG-1 Deletion Potentiates Thalamocortical Glutamatergic Inputs

The LFP in vivo data have shown that PRG-1 influences the development of spontaneous and sensory-evoked activity in the barrel cortex. Since functional analyses of specific synaptic connections, for instance thalamocortical glutamatergic synapses, are difficult to perform under in vivo conditions, we next applied whole-cell patch clamp methods in thalamocortical brain slices prepared from WT and PRG-1-KO mice (Agmon and Connors 1991; Schubert et al. 2003; Staiger et al. 2004) to study the question whether PRG-1 directly modulates thalamocortical inputs to barrel cortex already at P16–19. Patch clamp recordings from spiny stellate neurons in Layer 4 revealed a strong increase in the frequency of spontaneous PSCs in PRG-1-KO animals (17.7 ± 1.8 Hz, $n = 9$ cells) compared with WT mice (7.7 ± 0.8, $n = 10$, $P < 0.001$, unpaired Student's *t*-test, see Supplementary Fig. 3). These results demonstrate that PRG-1 deficiency potentiates spontaneous network activity in neocortical Layer 4 in the thalamocortical in vitro preparation.

Next we recorded evoked excitatory postsynaptic potentials (eEPSCs) from Layer 4 spiny stellate neurons elicited by electrical stimulation in the VPM of the thalamus. Significantly larger amplitudes of eEPSCs were observed in Layer 4 cells of KO animals (25 ± 4 pA, $n = 9$) compared with WT littermates (5.3 ± 1.1 pA, $n = 8$, $P < 0.001$, unpaired Student's *t*-test, Fig. 6*A*,*B*). In addition, the

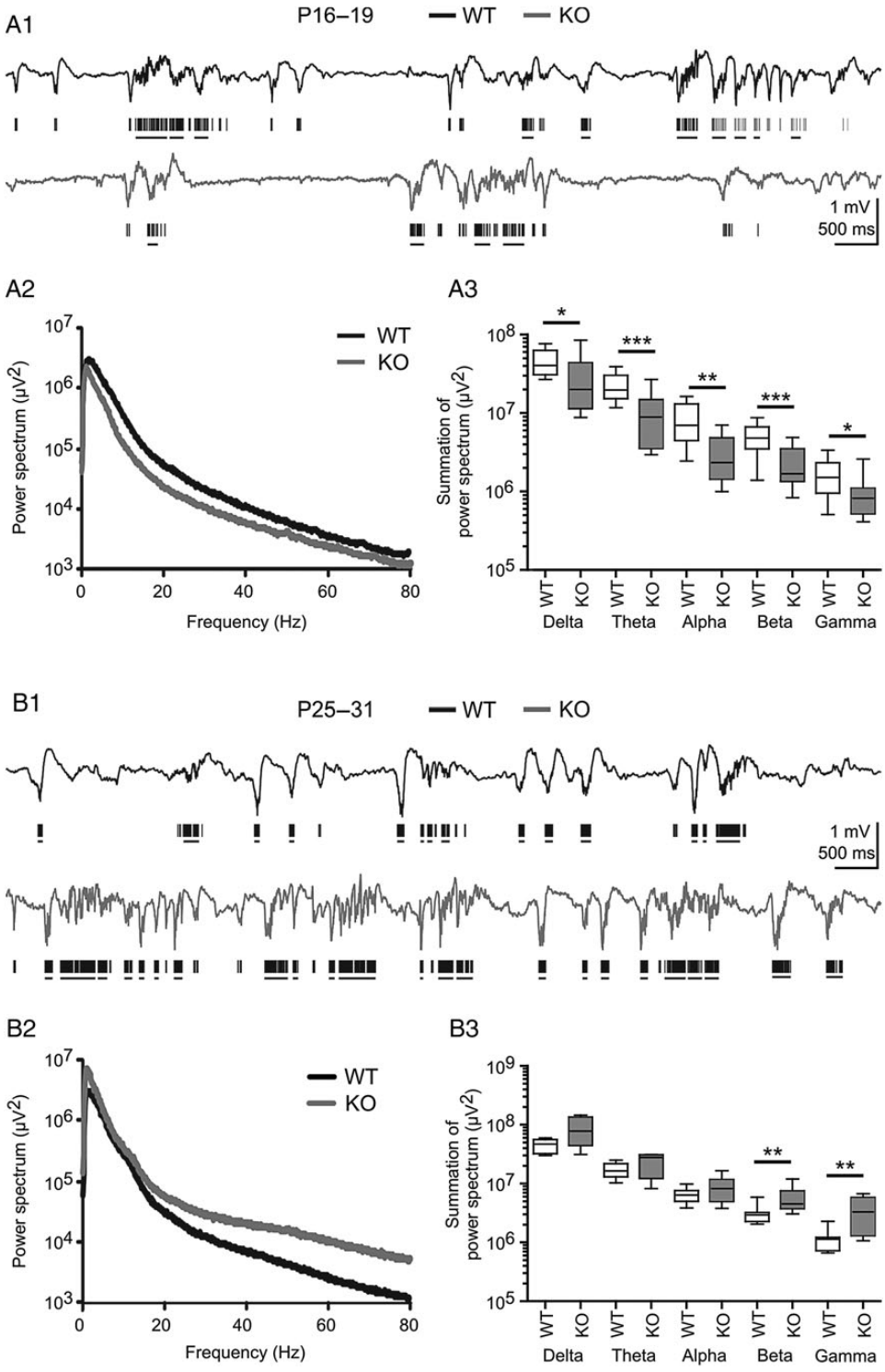

Figure 2. PRG-1 genetic ablation influences spontaneous neuronal activity in the somatosensory cortex in vivo. (A1) Representative traces showing 10 s in vivo recordings of spontaneous extracellular local field potentials (LFP) in P16–19 wild-type (WT, black) and PRG-1-KO (KO, gray) mouse. Corresponding multi-unit activity (MUA) is shown below the LFP traces. Horizontal lines below MUA traces display MUA bursts. (A2) Averaged power spectra of 30 min continuous LFP recordings from 12 barrels in 5 WT mice and 15 barrels in 7 PRG-1-KO mice. (A3) Box plots illustrating the power spectra in different frequency bands. (B1) Representative traces showing 10 s in vivo recordings of spontaneous LFPs in P25–31 WT (black) and PRG-1-KO (KO, gray) mouse and corresponding MUA with MUA bursts. (B2) Average power spectra of 30 min continuous LFP recordings from 10 barrels in 5 WT mice and 8 barrels in 4 KO mice. (B3) Box plot illustrating the power spectra in different frequency bands. Asterisks mark significant differences, $^{*}P < 0.05$, $^{**}P < 0.01$, and $^{***}P < 0.001$, Mann–Whitney–Wilcoxon test.

failure rate of eEPSCs, that is, percentage of trials in which the first electrical stimulus failed to elicit an eEPSC, was significantly higher in WT slices compared with KO ones (0.44 ± 0.09 and 0.16 ± 0.05, respectively, $P = 0.016$, unpaired Student's t-test, Fig. 6C), suggesting a presynaptic locus of PRG-1 action. To corroborate this finding, we applied a paired-pulse stimulation protocol.

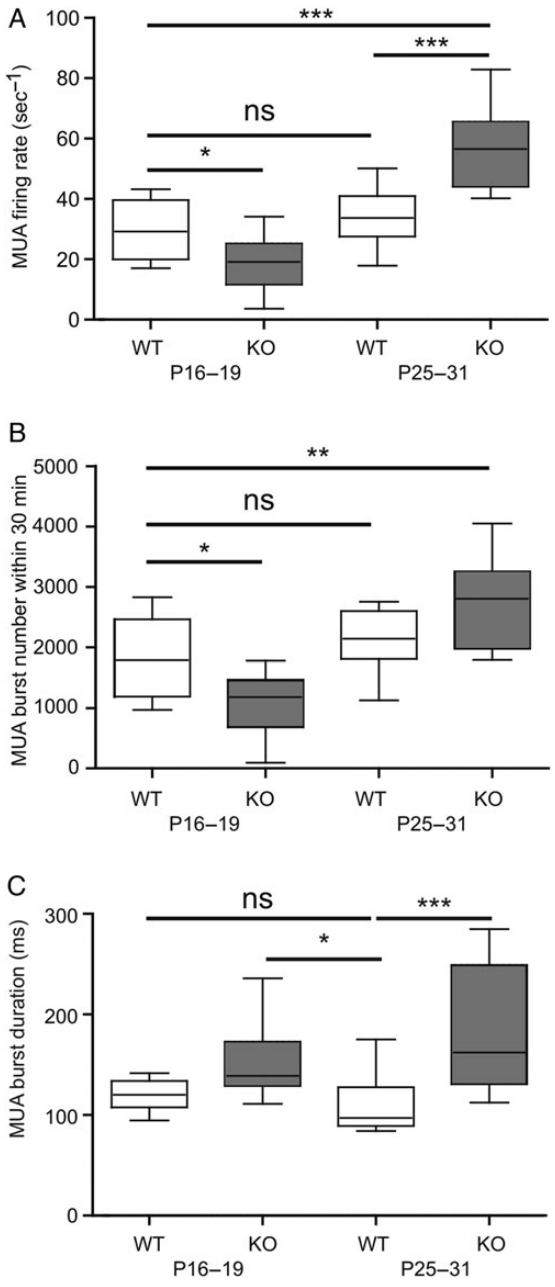

Figure 3. Genetic ablation of PRG-1 affects multiunit activity (MUA) in the somatosensory cortex in vivo. (*A–C*) Box plots showing spontaneous MUA firing rate (*A*), number of MUA bursts (*B*), and MUA burst duration (*C*) in WT and PRG-1-KO mice of the P16–19 and P25–31 age group. Statistical analyses were performed using 1-way ANOVA test followed by post hoc Tukey's multiple comparison test. Asterisks mark significant differences, $^{*}P < 0.05$, $^{**}P < 0.01$, $^{***}P < 0.001$, and ns, not significant.

If genetic ablation of PRG-1 facilitates presynaptic release probability, it should result in a decrease of the paired pulse ratio (PPR), that is, the mean amplitude of the second eEPSC divided by the mean amplitude of the first eEPSC. Indeed, the PPR was significantly smaller in cells of PRG-1-KO mice (at 50 ms ISI: 0.11 ± 0.04, $n = 9$) compared with WTs (0.67 ± 0.16, $n = 8$, $P = 0.003$, unpaired Student's *t*-test, Fig. 6*D*). However, not only presynaptic but also postsynaptic changes may result in an eEPSC amplitude increase and PPR reduction. Therefore, miniature EPSCs (mEPSCs) were recorded in the presence of TTX and gabazine (Fig. 7). mEPSCs are postsynaptic responses induced by the content of a single presynaptic vesicle. If PRG-1 presynaptically modulates synaptic transmission, its ablation should alter only mEPSC frequency, whereas a postsynaptic PRG-1 action should affect mEPSC amplitude. PRG-1 deletion significantly increased mEPSC frequency (KO 2.6 ± 0.2 Hz, $n = 11$) compared with WT mice (1.6 ± 0.2 Hz, $n = 12$, $P < 0.001$, unpaired Student's *t*-test, Fig. 7*A*,*B*). However, the mean mEPSC amplitudes did not differ between WT (6.3 ± 0.3 pA, $n = 12$) and PRG-1-KO mice (6.6 ± 0.4 pA, $n = 11$, $P = 0.58$, unpaired Student's *t*-test, Fig. 7*A*,*C*). Thus, we conclude that genetic ablation of PRG-1 results in a direct presynaptic strengthening of glutamatergic thalamocortical projections at P16–19.

Trimbuch et al. (2009) reported that PRG-1 in the hippocampus is located postsynaptically at glutamatergic synapses while PRG-1 action is mediated by presynaptic LPA_2 receptors. To elucidate whether postsynaptic re-expression of PRG-1 in PRG-1-KO neurons can abolish the observed potentiation of thalamocortical glutamatergic inputs in PRG-1-KO animals, we applied the in utero electroporation technique. This method allows a re-expression of the genetically ablated gene, in our case *prg-1*, in a small subpopulation of cells. We could easily identify the Layer 4 neurons with re-expressed PRG-1 by their GFP fluorescence and morphology (Fig. 8*A*). mEPSCs were recorded from GFP-positive, PRG-1 re-expressing and neighboring GFP-negative, PRG-1-KO cells (Fig. 8*B*). mEPSC frequency was significantly reduced (1.6 ± 0.1 Hz) in neurons re-expressing PRG-1 compared with PRG-1-KO cells (2.8 ± 0.2 Hz, $n = 11$ cells from 6 animals in both cases, $P < 0.001$, unpaired Student's *t*-test, Fig. 8*B*,*C*), but it did not change the mean mEPSC amplitude (6.9 ± 0.3 and 6.7 ± 0.3 pA in PRG-1-negative and PRG-1-positive neurons, respectively, $P = 0.62$, unpaired Student's *t*-test, Fig. 8*D*). These results demonstrate that postsynaptic PRG-1, that is, located in cortical Layer 4 stellate neurons, underlies the presynaptic augmentation of glutamatergic thalamocortical synaptic transmission in PRG-1-deficient barrel cortex already at P16–19.

Discussion

In this study, we have investigated with behavioral and in vivo and in vitro electrophysiological methods the functional role of PRG-1 in adolescent and adult mouse barrel cortex. Our main observations can be summarized as follows: 1) Genetic elimination of *prg-1* distorts sensory, but not motor function in adult animals. 2) In vivo, spontaneous network activity and evoked synaptic responses elicited by single whisker stimulation are facilitated in PRG-1-KO mice at P25–31, but not at P16–19. 3) In vitro, glutamatergic thalamocortical inputs onto Layer 4 neurons are potentiated in PRG-1-KO mice already at P16–19 due to a presynaptic augmentation of transmitter release. Our data strongly indicate that PRG-1 is required for the developmental, activity-dependent fine-tuning of sensory cortex function.

PRG-1 Deletion Affects Sensorimotor Performance and Sensory Perception

The beam walking/balance test and the Rota Rod test are well established and frequently used tests for motor phenotyping of rodents (Crawley and Paylor 1997; Carter et al. 2001). While the Rota Rod test, which consists in repetition of monotone, stereotypic movement sequences, is used to assess differences in motor performance, the beam walking/balance test is more sensitive for additional sensory processing in rodents, for example, examining their processing of balance and proprioception

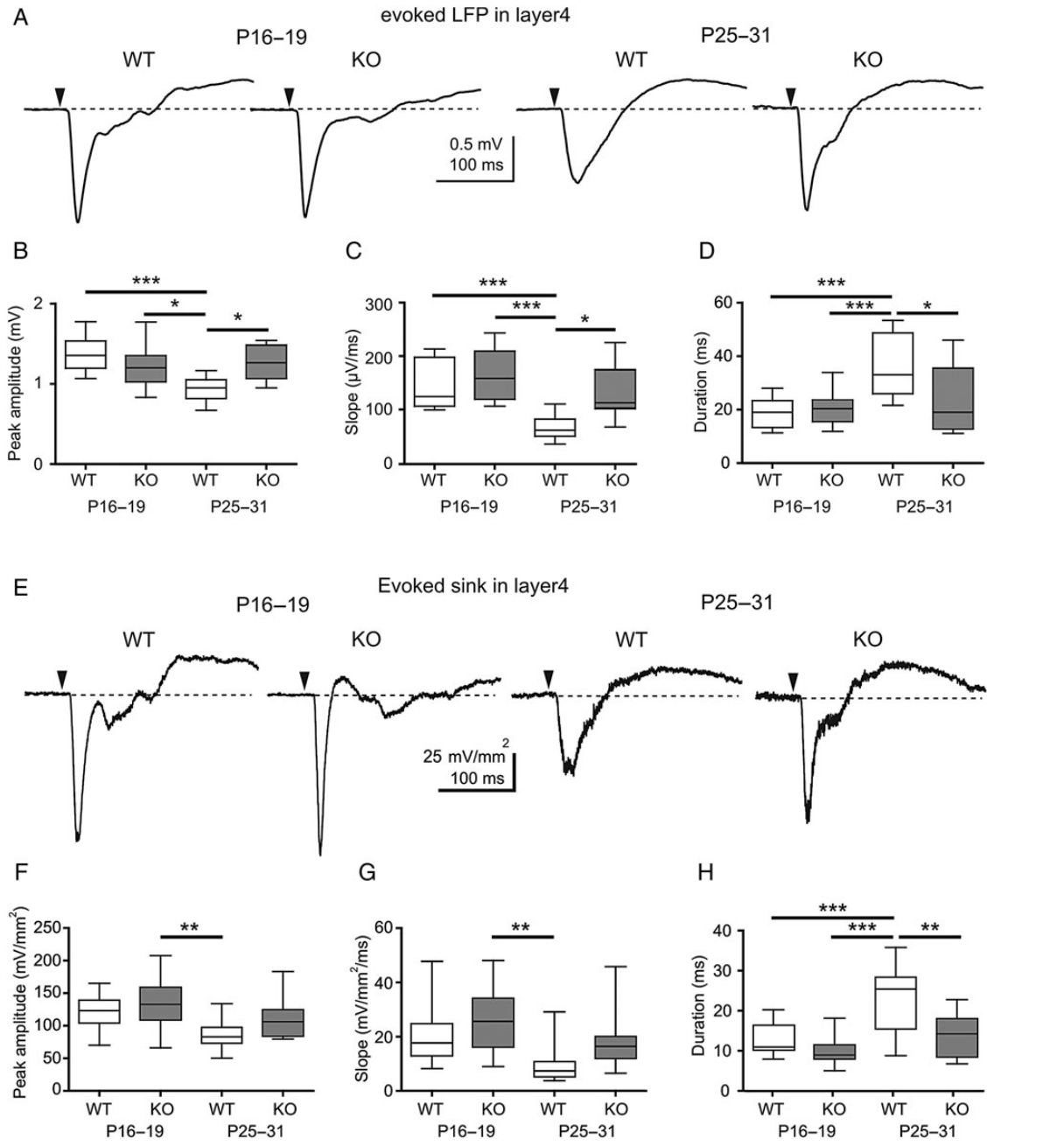

Figure 4. PRG-1 deletion prevents functional maturation of sensory-evoked responses in the somatosensory cortex in vivo. (*A*) Average of evoked LFP responses from P16–19 WT (12 barrels, 5 mice), P16–19 PRG-1-KO (15 barrels, mice, 7 mice), P25–31 WT (10 barrels, 5 mice), and P25–31 PRG-1-KO (8 barrels, 4 mice). The black arrowheads indicate the time point of mechanical single whisker stimulation. (*B–D*) Box plots showing the peak amplitude (*B*), slope (*C*), and duration (*D*) of the evoked responses in the 4 groups. (*E*) Average of evoked sink responses from P16–19 WT (12 barrels, 5 mice), P16–19 PRG-1-KO (15 barrels, 7 mice), P25–31 WT (10 barrels, 5 mice), and P25–31 PRG-1-KO (8 barrels, 4 mice). (*F–H*) Box plots showing the peak amplitude (*F*), slope (*G*), and duration (*H*) of the evoked sink responses in the 4 groups. Statistical analyses were performed using 1-way ANOVA test followed by Tukey's multiple comparison test. Asterisks mark significant differences, $^{*}P < 0.05$, $^{**}P < 0.01$, $^{***}P < 0.001$, and ns, not significant.

(Luong et al. 2011). Using the beam walking/balance test, we could detect specific deficits in the sensorimotor performance which were especially evident, when mice had to walk on the 5-mm-wide beam, which affords a higher level of sensory information processing. This assumption is further supported by direct assessment of whisker-related sensory perception showing a significant deficit in PRG-1 KO mice. Since tactile discrimination in rodents is specifically processed in the somatosensory barrel cortex (Garion et al. 2014), our results point to a distinct deficit in sensory processing in PRG-1 KO mice. Moreover, performing the Rota Rod test, where PRG-1 KO mice showed no deficits, we could rule out an impairment of basic motor functions. In terms of basic motor coordination, PRG-1 KO mice performed even better than their WT litters, which most probably reflects a strengthening of glutamatergic transmission and a higher neuronal excitability in the motor cortex upon PRG-1 deletion as reported for the hippocampus (Trimbuch et al. 2009). This is in line with recent data showing that alteration of the

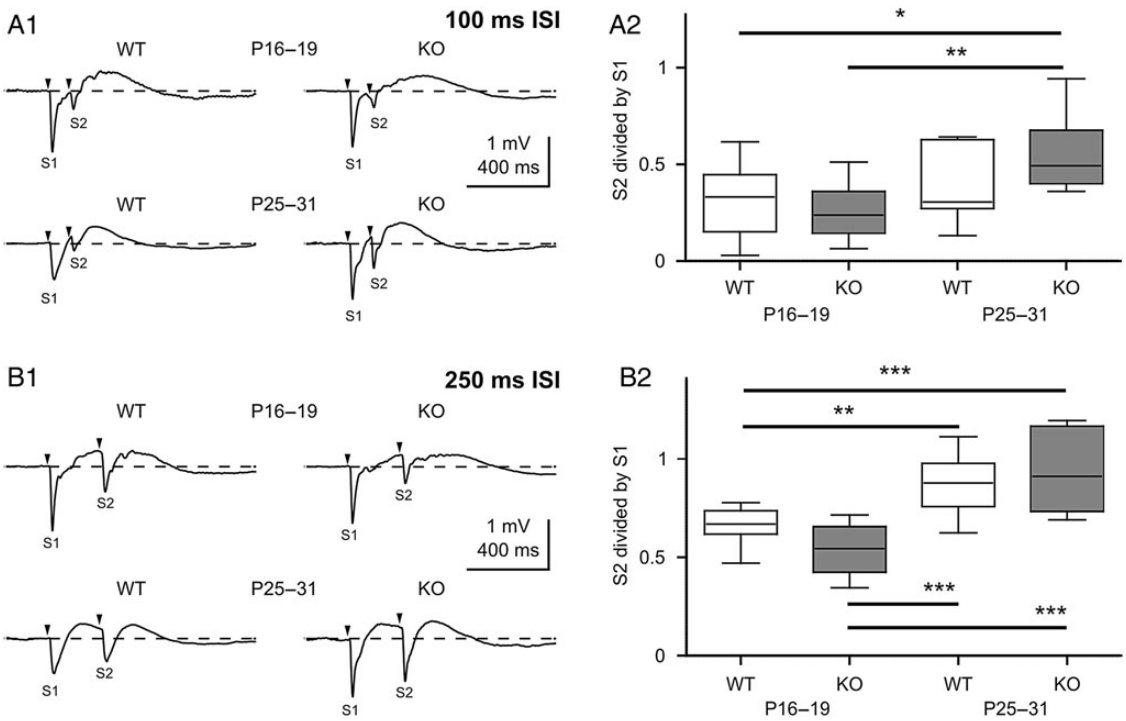

Figure 5. PRG-1-KO does not affect paired-pulse plasticity in vivo. (*A1*) Average of paired-pulse evoked responses at 100 ms inter-stimulus interval in 4 groups. (*A2*) Box plots showing corresponding S2/S1 ratios from *A1*. (*B1*) Average of paired-pulse evoked responses at 250 ms inter-stimulus interval. (*B2*) Box plots illustrating corresponding S2/S1 ratios from *B1*. Statistical analyses were performed using 1-way ANOVA test followed by Tukey's multiple comparison test. Asterisks mark significant differences, $^{*}P < 0.05$, $^{**}P < 0.01$, and $^{***}P < 0.001$.

glutamatergic transmission in the motor cortex may affect Rota Rod performance (Guimaraes et al. 2015). In sum, these data demonstrate that PRG-1 deficiency results in a specific deficit to integrate sensory information and its processing in PRG-1 KO mice.

Spontaneous Activity in PRG-1-Deficient Barrel Cortex

The deficit in sensorimotor performance of PRG-1-KO mice suggests that PRG-1 ablation modifies information processing in the somatosensory cortex. Therefore, we investigated functional alterations in the barrel cortex, a well-suited model to study intracortical processing of sensory information (for review, Feldmeyer et al. 2013). Spectral analysis of spontaneous LFP activity in P25-31 barrel cortex in vivo revealed a significant increase in the β and γ band power in PRG-1-KO mice (Fig. 2*B3*). In addition, MUA firing rate also demonstrated a strong increase in PRG-1-KO mice compared with WT littermates (Fig. 3*A*,*B*). Spectral analysis of LFP recordings performed in adolescent (P16–19) barrel cortex revealed a decrease in power at all frequency bands (Fig. 2*A3*), and this reduction was accompanied by a decrease in MUA firing rate (Fig. 3*A*,*B*). There was no significant difference between either power spectra of LFP recordings or MUAs in P16–19 and P25–31 WT animals. These results suggest that PRG-1 contributes to both diminishing of spontaneous activity at P16–19 and potentiation of spontaneous activity at P25–31 in PRG-1-KO animals. As gamma oscillations are suggested to represent an important mechanism of information processing during sensory perception and memory formation (Ainsworth et al. 2012; Ross et al. 2013), disturbances in cortical gamma activity in PRG-1-KO mice may underlie sensorimotor deficit of these animals in adulthood.

Evoked Sensory Responses in PRG-1-Deficient Barrel Cortex

Similar to the spontaneous activity, evoked LFP responses elicited by single whisker stimulation were also significantly larger in P25–31 PRG-1-KO barrel cortex compared with WT (Fig. 4*A–C*). The CSD analyses showed the trend that evoked current sinks were larger in P25–31 PRG-1-KO barrel cortex compared with WT, but this difference was not significant (Fig. 4*F*,*G*). However, in contrast to the spontaneous activity, this difference did not result from an enhancement of the evoked response in PRG-1-deficient mice. Neither amplitude nor duration of evoked LFP and sink responses in P16–19 WT, P16–19 PRG-1-KO, and P25–31 PRG-1-KO mice differed significantly. Our data demonstrate that during normal development (in WT mice) sensory-evoked responses in the barrel cortex become smaller and broader during the third and fourth postnatal week. However, this developmental transformation does not occur in the PRG-1-deficient mice corroborating the hypothesis of a maturation deficit in sensory information processing in these mice. In adult barrel cortex, sensory-evoked responses in Layer 4 are shaped by potent feedforward GABAergic inhibition (Gabernet et al. 2005; Daw, Scott, et al. 2007). As GABAergic neurons do not express PRG-1 (Trimbuch et al. 2009), the strength of this feedforward GABAergic inhibition should not be influenced by PRG-1 deletion. Unchanged S2/S1 ratio of sensory-evoked responses in vivo (Fig. 5) indirectly supports the suggestion that the evoked GABAergic responses are not changed in PRG-1-KO mice. More likely, PRG-1 deletion causes a potentiation of glutamatergic thalamocortical inputs leading to an increase of sensory-evoked responses and spontaneous activity in the barrel cortex. Interestingly, our in vitro data show that the thalamocortical input to Layer 4 in PRG-1-KO

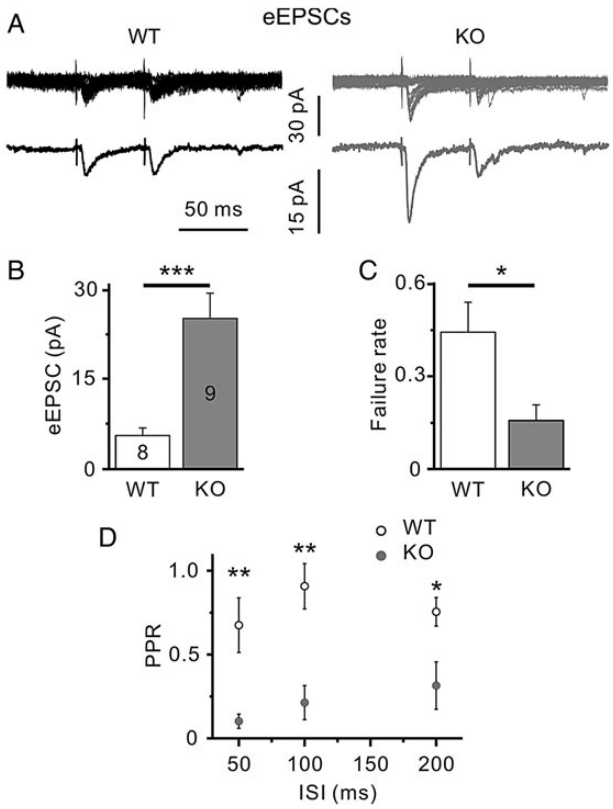

Figure 6. PRG-1-KO mice show increased evoked (e)EPSCs in somatosensory cortex in vitro. (*A*) Representative eEPSCs recorded from Layer 4 spiny stellate neurons in WT (left) and KO (right panel) mice. eEPSCs were elicited by paired-pulse electrical stimulation in the ventrobasal thalamus. Upper traces demonstrate original eEPSCs (20 in both cases); lower traces show the averaged responses. (*B–D*) Significantly larger eEPSC amplitudes (*B*), smaller failure rates (*C*), and smaller paired-pulse ratios (at 50, 100, and 200 ms ISIs; *D*) were observed in PRG-1-KO mice compared with WT littermates. Numbers indicate number of cells. *, **, and ***, $P < 0.05$, $P < 0.01$, and $P < 0.001$, respectively, unpaired Student's *t*-test.

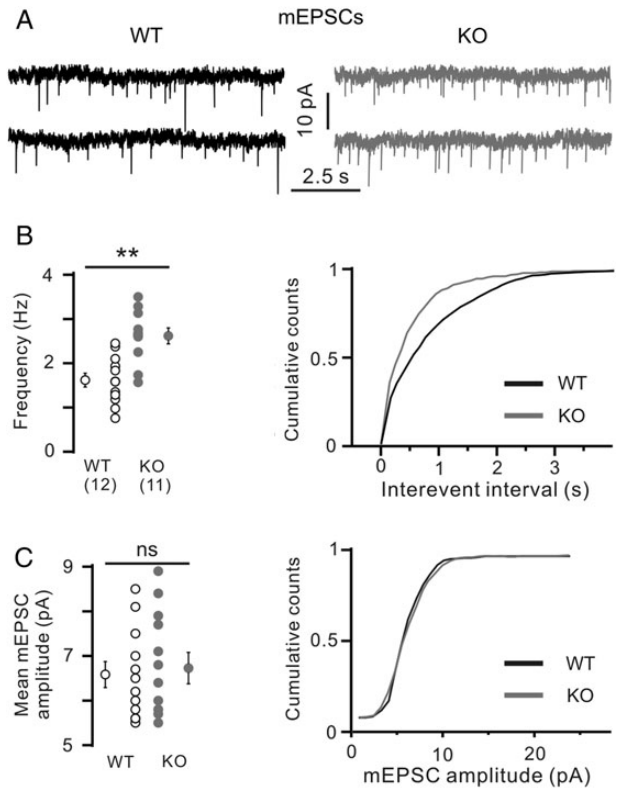

Figure 7. Layer 4 spiny stellate cells in PRG-1-KO mice demonstrate increased mEPSC frequency. (*A*) Representative mEPSCs recorded in WT (left) and KO (right panel) mice. (*B*) Significantly higher frequency of mEPSCs observed in KO mice compared with WT littermates. Left panel shows mean values. Right panel shows cumulative distribution of interevent intervals. (*C*) Mean mEPSC amplitude did not vary between WT and PRG-1-KO groups. Numbers in (*B*) indicate number of cells. **$P < 0.01$, ns, not significant, unpaired Student's *t*-test.

animals is potentiated already at P16–19 (Fig. 6), whereas in vivo neuronal activity at P16–19 is reduced. This discrepancy suggests the existence of compensatory mechanism(s) which can prevent hyperexcitation, but this mechanism(s) appears to become exhausted at P25–31.

PRG-1 Modulates Thalamocortical Synapses

PRG-1 is expressed in various brain regions, including the cerebral cortex (Tokumitsu et al. 2010). In the barrel cortex, the highest levels of PRG-1 expression are observed in Layer 4 (Vogt et al 2015; see Supplementary Fig. 1). The barrel cortex contains the topographic representation of the whiskers, and Layer 4 receives the majority of the thalamocortical inputs (Castro-Alamancos and Connors 1997; Daw, Ashby, et al. 2007). In the hippocampus, PRG-1 KO has been reported to selectively potentiate glutamatergic synaptic transmission, while GABAergic responses were not affected (Trimbuch et al. 2009). As thalamocortical projections to Layer 4 are glutamatergic and synapse on glutamatergic, PRG-1-expressing spiny stellate and pyramidal cells of Layer 4, we asked whether the strength of these connections is modulated by PRG-1. Indeed, PRG-1-deficient spiny stellate cells demonstrated larger eEPSCs elicited by electrical stimulation in the thalamic VPM. In addition, PPR of eEPSCs was decreased. It is generally believed that a decrease in PPR reflects an increase in presynaptic release probability, although postsynaptic changes such as desensitization of postsynaptic receptors can also contribute to this (Kirischuk et al. 2002; Zucker and Regehr 2002). However, as PPR was decreased at 3 ISIs studied (50, 100, and 200 ms, Fig. 6*D*), a contribution of postsynaptic receptor desensitization is rather unlikely. In addition, the decrease in failure rate observed in PRG-1 KO mice indicates a presynaptic locus of PRG-1-mediated action. The observed increase in mEPSC frequency (Fig. 7) can result either from an elevated presynaptic release probability or increased number of synapses, or a combination of both mechanisms. Unfortunately, we cannot distinguish between these possibilities. However, the number of glutamatergic synapses in the hippocampus was shown to be unchanged in PRG1-deficient mice (Trimbuch et al. 2009), also indicating that PRG-1 modulates presynaptic release probability. Finally, because re-expression of PRG-1 in constitutively PRG-1-deficient neurons decreased mEPSC frequency to control (WT) level, we conclude that PRG-1, located postsynaptically to cortical spiny stellate cells, modulates presynaptic release probability of glutamatergic thalamocortical synapses already at P16–19.

Mechanism of PRG-1 Action

Due to its homology to LPPs, PRG-1 was originally described as a new member of the LPP family, able to interact with LPA (Brauer et al. 2003; Sigal et al. 2005). However, although LPA-binding

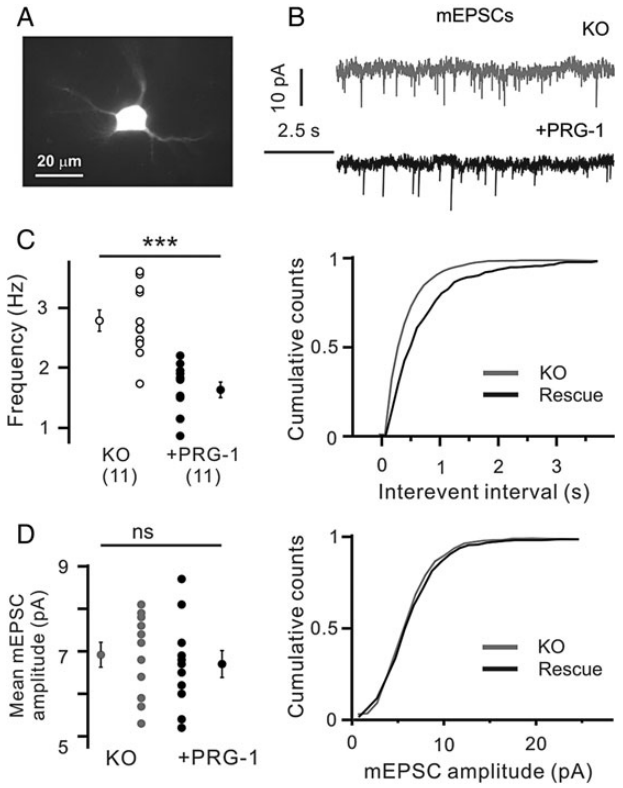

Figure 8. Re-expression of PRG-1 in a subset of cells in constitutive PRG-1-KO mice influenced the frequency of mEPSCs. (*A*) Representative image of in utero electroporated Layer 4 spiny stellate cell. (*B*) Representative recordings of mEPSCs from PRG-1-deficient (KO) and PRG-1-expressing Layer 4 spiny stellate cells. (*C*,*D*) Re-constitution of PRG-1 expression reduced the frequency of mEPSCs (*C*) and did not alter the mean amplitude of mEPSCs (*D*). Numbers in (*B*) indicate number of cells. ***$P < 0.001$; ns, not significant, unpaired Student's *t*-test.

motives are conserved, in contrast to LPPs, PRG-1 lacks conserved amino acids critical for phosphatase activity (Brindley 2004). In our previous work, we could show that PRG-1, which is located at the postsynaptic density of glutamatergic synapses, interacts with phospholipids leading to their internalization, thereby modulating phospholipid signaling (Trimbuch et al. 2009). Identifying LPA_2-receptor (LPA_2-R) expression on glutamatergic presynaptic terminals and their role in mEPSC modulation upon LPA stimulation led to description of the LPA/LPA_2-R/PRG-1 axis where PRG-1 modulates synaptic LPA action at presynaptic LPA_2-Rs, thereby influencing glutamate release (Trimbuch et al. 2009). The observation that LPA_2/PRG-1 double KO mice displayed normal glutamatergic transmission and did not show any sign of over-excitability in vitro and in vivo, as present in PRG-1-deficient animals, supported the described LPA/LPA_2-R/PRG-1 axis. However, an approximately linear relationship between protein expression and its electrophysiological actions argues for a specific modulatory function of PRG-1 (Trimbuch et al. 2009). While the exact mechanism of PRG-1 function is not fully elucidated, PRG-1 has been shown to bind to calmodulin in a Ca^{2+}-dependent manner suggesting that postsynaptic activity/Ca^{2+} dynamics may influence PRG-1 (Tokumitsu et al. 2010). These data suggest that PRG-1 control of extrasynaptic LPA concentration may be dynamic and activity-regulated. Activity-dependent elevation of postsynaptic Ca^{2+} concentration, which is generally believed to regulate synaptic transmission through a variety of postsynaptic mechanisms, could thus in addition influence glutamatergic transmission via modulation of postsynaptic PRG-1 function affecting extrasynaptic LPA levels and thereby presynaptic LPA_2-R activation.

Postsynaptic modulation of PRG-1 activity might also explain the temporal discrepancy between in vivo and in vitro data. Lack of postsynaptic PRG-1 may only moderately, although significantly, enhance the release probability at thalamocortical glutamatergic synapses at P16–19. A developmental increase of thalamocortical information transfer, presumably occurring between P19 and P25, may potentiate postsynaptic activity in Layer 4 spiny stellate cells and in turn influence postsynaptic PRG-1 activity. Modified PRG-1 activity acting on the LPA/LPA_2-R pathway may result in an increased presynaptic release probability, providing thereby a positive feedback mechanism. High level of thalamic activity will boost neuronal activity in the barrel cortex, which was indeed observed in PRG-1-KO mice (epileptic seizures). Moderately enhanced thalamic input will also increase spontaneous activity and sensory evoked responses in the barrel cortex at P25–31 but will not result in an epileptic form of activity. However, this hyperexcited state will interfere with the developmental, activity-dependent fine tuning of cortical synaptic connectivity.

Supplementary Material

Supplementary material can be found at: http://www.cercor.oxfordjournals.org/.

Funding

This study was supported by a grant of the Stiftung Rheinland-Pfalz für Innovation 961-386261/955 to S.K., DFG grants to J.V., R.N., and H.J.L. (SFB 1080), and an ERC-AG "LiPsyD" to R.N. Funding to pay the Open Access publication charges for this article was provided by European Research Council (ERC), Advanced Grant to RN LiPsyD.

Notes

The excellent technical assistance of Mrs Beate Krumm is highly appreciated. *Conflict of Interest*: None declared.

References

Agmon A, Connors BW. 1991. Thalamocortical responses of mouse somatosensory (barrel) cortex in vitro. Neuroscience. 41:365–379.

Ainsworth M, Lee S, Cunningham MO, Traub RD, Kopell NJ, Whittington MA. 2012. Rates and rhythms: a synergistic view of frequency and temporal coding in neuronal networks. Neuron. 75:572–583.

Beierlein M, Gibson JR, Connors BW. 2003. Two dynamically distinct inhibitory networks in layer 4 of the neocortex. J Neurophysiol. 90:2987–3000.

Brauer AU, Savaskan NE, Kuhn H, Prehn S, Ninnemann O, Nitsch R. 2003. A new phospholipid phosphatase, PRG-1, is involved in axon growth and regenerative sprouting. Nat Neurosci. 6:572–578.

Brindley DN. 2004. Lipid phosphate phosphatases and related proteins: signaling functions in development, cell division, and cancer. J Cell Biochem. 92:900–912.

Carter RJ, Morton J, Dunnett SB. 2001. Motor coordination and balance in rodents. Curr Protoc Neurosci. 15:8.12.1–8.12.14.

Castro-Alamancos MA, Connors BW. 1997. Thalamocortical synapses. Prog Neurobiol. 51:581–606.

Crawley JN, Paylor R. 1997. A proposed test battery and constellations of specific behavioral paradigms to investigate the behavioral phenotypes of transgenic and knockout mice. Horm Behav. 31:197–211.

Daw MI, Ashby MC, Isaac JT. 2007. Coordinated developmental recruitment of latent fast spiking interneurons in layer IV barrel cortex. Nat Neurosci. 10:453–461.

Daw MI, Scott HL, Isaac JT. 2007. Developmental synaptic plasticity at the thalamocortical input to barrel cortex: mechanisms and roles. Mol Cell Neurosci. 34:493–502.

Feldman DE, Nicoll RA, Malenka RC. 1999. Synaptic plasticity at thalamocortical synapses in developing rat somatosensory cortex: LTP, LTD, and silent synapses. J Neurobiol. 41:92–101.

Feldmeyer D, Brecht M, Helmchen F, Petersen CC, Poulet JF, Staiger JF, Luhmann HJ, Schwarz C. 2013. Barrel cortex function. Prog Neurobiol. 103:3–27.

Fox K, Schlaggar BL, Glazewski S, O'Leary DD. 1996. Glutamate receptor blockade at cortical synapses disrupts development of thalamocortical and columnar organization in somatosensory cortex. Proc Natl Acad Sci USA. 93:5584–5589.

Freeman JA, Nicholson C. 1975. Experimental optimization of current-source-density technique for anuran cerebellum. J Neurophysiol. 38:369–382.

Fukushima N, Weiner JA, Kaushal D, Contos JJ, Rehen SK, Kingsbury MA, Kim KY, Chun J. 2002. Lysophosphatidic acid influences the morphology and motility of young, postmitotic cortical neurons. Mol Cell Neurosci. 20:271–282.

Gabernet L, Jadhav SP, Feldman DE, Carandini M, Scanziani M. 2005. Somatosensory integration controlled by dynamic thalamocortical feed-forward inhibition. Neuron. 48:315–327.

Garion L, Dubin U, Rubin Y, Khateb M, Schiller Y, Azouz R, Schiller J. 2014. Texture coarseness responsive neurons and their mapping in layer 2-3 of the rat barrel cortex in vivo. eLife 3:e03405.

Guimaraes IM, Carvalho TG, Ferguson SS, Pereira GS, Ribeiro FM. 2015. The metabotropic glutamate receptor 5 role on motor behavior involves specific neural substrates. Mol Brain. 8:24.

Kingsbury MA, Rehen SK, Contos JJ, Higgins CM, Chun J. 2003. Non-proliferative effects of lysophosphatidic acid enhance cortical growth and folding. Nat Neurosci. 6:1292–1299.

Kirischuk S, Clements JD, Grantyn R. 2002. Presynaptic and postsynaptic mechanisms underlie paired pulse depression at single GABAergic boutons in rat collicular cultures. J Physiol. 543:99–116.

Kirmse K, Dvorzhak A, Henneberger C, Grantyn R, Kirischuk S. 2007. Cajal-Retzius cells in the mouse neocortex receive two types of pre- and postsynaptically distinct GABAergic inputs. J Physiol. 585:881–895.

Krupa DJ, Brisben AJ, Nicolelis MA. 2001. A multi-channel whisker stimulator for producing spatiotemporally complex tactile stimuli. J Neurosci Methods. 104:199–208.

Luong TN, Carlisle HJ, Southwell A, Patterson PH. 2011. Assessment of motor balance and coordination in mice using the balance beam. J Vis Exp. 49:2376.

Malenka RC. 2003. The long-term potential of LTP. Nat Rev Neurosci. 4:923–926.

Morita T, Kang H, Wolfe J, Jadhav SP, Feldman DE. 2011. Psychometric curve and behavioral strategies for whisker-based texture discrimination in rats. PLoS One. 6:e20437.

Ross B, Jamali S, Miyazaki T, Fujioka T. 2013. Synchronization of beta and gamma oscillations in the somatosensory evoked neuromagnetic steady-state response. Exp Neurol. 245:40–51.

Rowland NE. 2007. Food or fluid restriction in common laboratory animals: balancing welfare considerations with scientific inquiry. Comp Med. 57:149–160.

Schubert D, Kötter R, Zilles K, Luhmann HJ, Staiger JF. 2003. Cell type-specific circuits of cortical layer IV spiny neurons. J Neurosci. 23:2961–2970.

Shiotsuki H, Yoshimi K, Shimo Y, Funayama M, Takamatsu Y, Ikeda K, Takahashi R, Kitazawa S, Hattori N. 2010. A rotarod test for evaluation of motor skill learning. J Neurosci Methods. 189:180–185.

Sigal YJ, McDermott MI, Morris AJ. 2005. Integral membrane lipid phosphatases/phosphotransferases: common structure and diverse functions. Biochem J. 387:281–293.

Staiger JF, Flagmeyer I, Schubert D, Zilles K, Kötter R, Luhmann HJ. 2004. Functional diversity of layer IV spiny neurons in rat somatosensory cortex: quantitative morphology of electrophysiologically characterized and biocytin labeled cells. Cereb Cortex. 14:690–701.

Tokumitsu H, Hatano N, Tsuchiya M, Yurimoto S, Fujimoto T, Ohara N, Kobayashi R, Sakagami H. 2010. Identification and characterization of PRG-1 as a neuronal calmodulin-binding protein. Biochem J. 431:81–91.

Trimbuch T, Beed P, Vogt J, Schuchmann S, Maier N, Kintscher M, Breustedt J, Schuelke M, Streu N, Kieselmann O, et al. 2009. Synaptic PRG-1 modulates excitatory transmission via lipid phosphate-mediated signaling. Cell. 138:1222–1235.

van Leeuwen FN, Giepmans BN, van Meeteren LA, Moolenaar WH. 2003. Lysophosphatidic acid: mitogen and motility factor. Biochem Soc Trans. 31:1209–1212.

Vogt J, Yang JW, Mobascher A, Cheng J, Li Y, Liu X, Baumgart J, Thalman C, Kirischuk S, Unichenko P, et al. 2015. Molecular cause and functional impact of altered synaptic lipid signaling due to a prg-1 gene SNP. EMBO Mol Med. 8:25–38.

Yang JW, Hanganu-Opatz IL, Sun JJ, Luhmann HJ. 2009. Three patterns of oscillatory activity differentially synchronize developing neocortical networks in vivo. J Neurosci. 29:9011–9025.

Zucker RS, Regehr WG. 2002. Short-term synaptic plasticity. Annu Rev Physiol. 64:355–405.